

Dual-Targeted Nanoreactors and Prodrugs: Hydrogen Peroxide Triggers Oxidative Damage and Prodrug Activation for Synergistic Elimination of Cancer Cells

Seong-Min Jo, Hyeong Seok Kim, Miae Won, Carole Champanhac, Jong Seung Kim,*
Frederik R. Wurm,* and Katharina Landfester*

Synergistic strategies by combining nanoreactors and prodrugs hold tremendous potential in anticancer treatment. However, precise death of target cancer cells remains a significant challenge due to the absence of an elaborate cancer targeting strategy. Here, a dual-targeting approach that combines the action of H₂O₂-producing folate receptor-targeted nanoreactors with a cyclooxygenase-2 (COX-2) targeted prodrug is reported. A folate-modified silica nanoreactor encapsulating glucose oxidase (GOX) is prepared to generate H₂O₂, which induces oxidative stress and allows the activation of the prodrug by targeted intracellular delivery. A novel prodrug bearing both COX-2 targeting Celecoxib and SN-38 anticancer agent with an H₂O₂-cleavable thioketal linker to activate the drug is presented. By dual-targeting, the generated H₂O₂ from GOX triggers the cleavage of a thioketal linker in the prodrug to produce the active form of the SN-38 anticancer drug in cancer cells inducing synergistic cell death. This dual-targeting strategy with a synergistic potency can aid in developing selective and effective anticancer therapeutics.

Previous studies used glucose oxidase (GOX)-loaded nanoreactors that produce H₂O₂ by consuming glucose and oxygen, leading to oxidative destruction of tumor cells.^[10–14] As glucose is abundant and not depleted in our body, the GOX-loaded nanoreactors would ensure the sustainable therapeutic effects. The produced H₂O₂ or the resulting hypoxia can further activate secondary anticancer agents (e.g., prodrugs, radical precursors).^[14–16] As H₂O₂-triggered prodrugs, modified doxorubicin or tirapazamine, polymerized camptothecin, or hypoxic-activated AQ4N have been proposed.^[17–19] The combination of non-targeted nanoreactors and non-guided prodrugs has been well studied but showed non-selective, random cytotoxicity toward both cancer and normal cells. Only

functionalized with targeting groups on the nanoreactors^[20–22] or prodrugs^[23–25] that selective cytotoxicity were achieved. However, such dual-targeting of both nanoreactors and prodrugs for more selective and effective anticancer strategy has not been explored to date and will be presented here for the first time.

Cyclooxygenase-2 (COX-2) is a promising intracellular target that is overexpressed in various cancer cells.^[26,27] It is involved in the conversion of arachidonic acid to prostaglandin H₂ and E₂, which is expressed in inflammation. We have previously used indomethacin as a representative cyclooxygenase antagonist that enables not only to guide COX-2 positive cells but to lead to the blockade of angiogenesis^[28] or inflammation.^[23–28]

1. Introduction

Synergistic chemotherapy that combines nanoreactors with prodrugs is a novel strategy for high efficacy and lower side effects to treat cancer^[1–4] Conventional nanomedicine or direct medication of plain drugs relies on the continuous injection of disposable nanocarriers or active anticancer drugs. It usually suffers from high dosages of drugs and poor compliance because of lacking selectivity toward cancer cells over normal cells.^[5–8] In contrast, targeted nanoreactors can produce anticancer agents selectively inside the tumor tissue with high efficiency while keeping low toxicity to normal tissue.^[9]

S.-M. Jo, C. Champanhac, F. R. Wurm, K. Landfester
Department of Physical Chemistry of Polymers
Max Planck Institute for Polymer Research
Ackermannweg 10, 55128 Mainz, Germany
E-mail: landfester@mpip-mainz.mpg.de

 The ORCID identification number(s) for the author(s) of this article can be found under <https://doi.org/10.1002/adfm.202200791>.

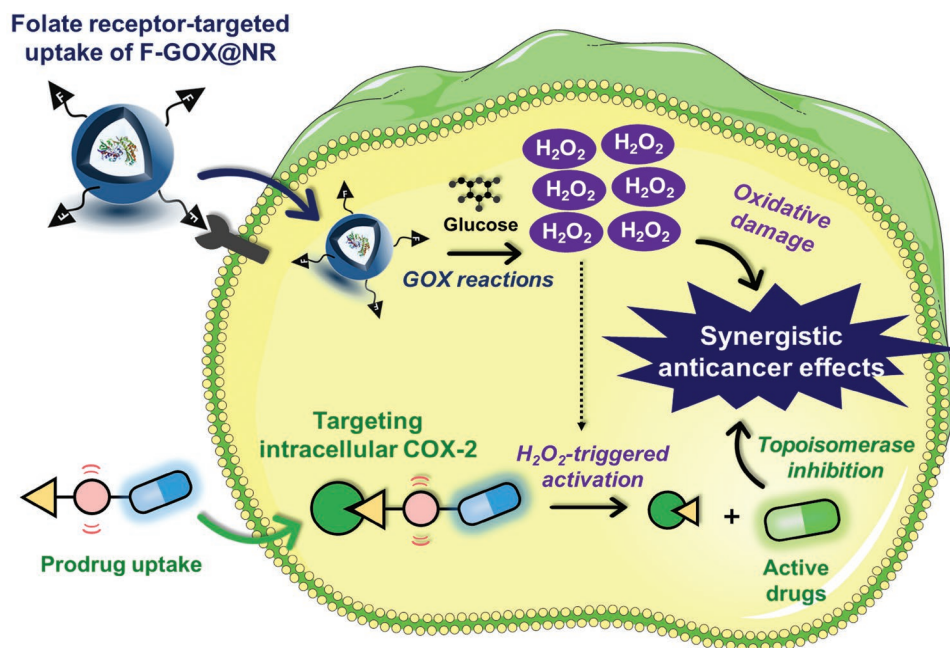
© 2022 The Authors. Advanced Functional Materials published by Wiley-VCH GmbH. This is an open access article under the terms of the Creative Commons Attribution-NonCommercial License, which permits use, distribution and reproduction in any medium, provided the original work is properly cited and is not used for commercial purposes.

^[†]Present address: Advanced Functional Polymers Center, Korea Research Institute of Chemical Technology, Daejeon 34114, Korea

DOI: 10.1002/adfm.202200791

H. S. Kim,^[†] M. Won, J. S. Kim
Department of Chemistry
Korea University
Seoul 02841, Republic of Korea
E-mail: jongskim@korea.ac.kr

F. R. Wurm
Sustainable Polymer Chemistry Group
MESA+ Institute for Nanotechnology
Faculty of Science and Technology
Universiteit Twente
PO Box 217, Enschede 7500, Netherlands
E-mail: f.r.wurm@utwente.nl



Scheme 1. Schematic illustration for dual-targeting and synergistic cytotoxicity by folate-modified H_2O_2 -generating nanoreactors (F-GOX@NR) and COX-2 targeting celecoxib/SN-38 prodrug 5. The uptake of nanoreactors occurs to the folate receptor-positive cells, producing H_2O_2 inside the cells, leading to oxidative cell death. The prodrug binds to intracellular COX-2, then, activated by H_2O_2 and leads to topoisomerase inhibition-mediated cell death. Two targeting mechanisms allow the accumulation of two anticancer agents together. A synergistic effect of the combination only follows for cells carrying both the folate receptor and COX-2.

Celecoxib is a well-known COX-2 targeting drug and showed better targeting toward COX-2 compared to indomethacin.

The folate receptor targeting strategy had been used in various drug delivery systems for cancer therapeutics.^[29–31] Targeted nanocarriers with loaded drugs are widely studied in cancer nanomedicine due to enabling specific eradication of tumors. Nevertheless, only a few studies were reported for targeted delivery of nanoreactors for GOX.^[20,32]

Here, we report a dual-targeting strategy using H_2O_2 -generating nanoreactors and ROS-activated prodrugs to enhance the potency and specificity for anticancer treatment with a potential high synergy. This dual-targeting strategy aims to lead the effective oncolysis by using a combination of the folate receptor-targeted nanoreactor loaded with GOX and the COX-2-binding prodrug (Scheme 1). The folate-modified and H_2O_2 -generating nanoreactor (F-GOX@NR) is rapidly and selectively transported into the folate receptor-positive cancer cells and generates H_2O_2 inside the cells by consuming only glucose. The generated H_2O_2 induces cytotoxicity by oxidation, glucose starvation, and apoptotic or necrotic signaling activation.^[33–38] In parallel, a prodrug of celecoxib/SN-38 (named “5”) binds to an intracellular COX-2 with its inactive form, which might help the accumulation in cytoplasm preventing rapid nuclei transportation and non-specific cell death. The H_2O_2 cleaves the thioketal linkers in 5, followed by the activated drug (SN-38) induces the cell death by inhibiting topoisomerase.^[39,40] This process occurs much faster at high H_2O_2 levels induced by F-GOX@NR, than intracellular H_2O_2 levels in normal range. With the dual-targeting of the folate receptors by F-GOX@NR and COX-2 by 5, we achieved a synergistic effect which led to significantly low IC_{50} -values compared to for 5 alone or its building blocks (SN-38 or celecoxib). Such synergistic and selective cytotoxicity might lead to customized and more effective anticancer

therapies against severe forms of cancer with fewer side effects in the future.

2. Results and Discussion

2.1. Design of Folate Receptor-Targeted and GOX-Loaded Nanoreactors (F-GOX@NR)

2.1.1. GOX-Loaded Nanoreactors (GOX@NR)

Many enzymes including GOX are unstable in biological environments, immunogenic, and exhibit low cellular uptake, making them unattractive to be used in biomedicine. Encapsulation of enzymes, for example, into silica nanoparticles, increased their stability and protection against proteolysis, which can increase their bioavailability.^[13,41,42] We encapsulated and covalently attached GOX into semipermeable silica nanoparticles (i.e., GOX@NR) by a one-pot sol-gel process using tetraethoxysiloxane (TEOS) and (3-Aminopropyl)trimethoxysilane (APTMS) as precursors.^[43–45] Potassium fluoride (F^-) was used as the catalyst for sol-gel reactions (Figure 1a), which preserves the enzymatic activity and secondary structure of GOX at a pH of ≈ 7.4 during the synthesis.^[44,45] GOX was covalently attached to the amino groups of APTMS via the reaction of NHS (*N*-hydroxysuccinimide) with EDC (1-ethyl-3-(3-dimethylaminopropyl)carbodiimide) (Figure 1a). The GOX@NR with diameters of ca. 60 nm were visualized by transmission electron microscopy (TEM) (Figure 1b). Detailed characterization of GOX@NR by dynamic light scattering for the size and size distribution, solid-state ^{29}Si magic-angle spinning (MAS) NMR spectroscopy for the silica linkages, and thermal gravimetric

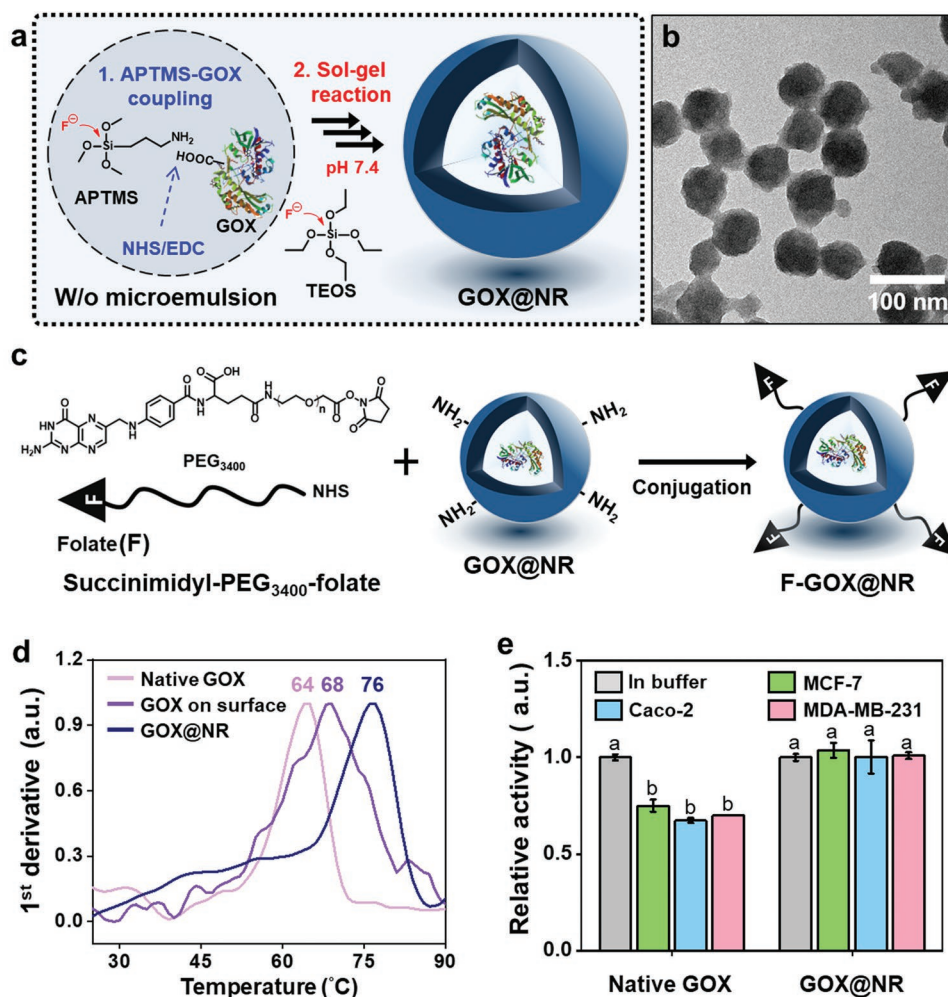


Figure 1. Synthesis and characterization of GOX@NR. a) Sol-gel process in microemulsion to prepare GOX@NR. An aqueous solution of GOX, KF, and APTMS are dispersed in cyclohexane/hexanol. The sol-gel reaction was initiated by adding TEOS. b) TEM image of GOX@NR. c) Functionalization of GOX@NR with folate-functionalized PEG by NHS (F-GOX@NR). d) NanoDSF thermogram of native GOX, GOX on surface, and GOX@NR proving increased thermal stability after encapsulation. e) Enzymatic activity of GOX and GOX@NR in different cell lysates in solution (data represented as mean \pm SEM ($n = 3$)). Statistical significance was determined by a one-way ANOVA test with a post-hoc Bonferroni test. Different letters (e.g., a, b) signify datasets that are statistically distinct ($p < 0.05$).

analysis (TGA) for the enzyme-contents determination are described in Figures S1–S3, Supporting Information. From thermogravimetry, GOX@NR showed a further mass loss of $\approx 12\%$ compared to empty silica nanoparticles indicating an encapsulation efficiency of $\approx 97\%$ (0.78 mg GOX in 6.5 mg nanoreactors; the initial amount of GOX in the reaction mixture was 0.8 mg). With 1.6 g cm^{-3} , GOX@NR exhibited a lower density than empty silica nanoparticles with 1.8 g cm^{-3} due to the encapsulated GOX (note: the average density of proteins is $\approx 1.4 \text{ g cm}^{-3}$).^[46] We estimated that 260 ± 17 GOX molecules were entrapped per nanoreactor, which was calculated by a combination of the density difference, radius ($r = 35 \text{ nm}$, from TEM), and mass of the loaded GOX (12%) in each nanoreactor (details can be found in the Supporting Information). The enzymatic activity of GOX@NR was determined by the Amplex red fluorescence assay. Based on the Michaelis-Menten kinetics, GOX@NR exhibited an enzymatic activity of $74 \pm 5 \mu\text{M}^{-1} \cdot \text{s}^{-1}$ (k_{cat}/K_m) (vs native GOX $244 \pm 10 \mu\text{M}^{-1} \cdot \text{s}^{-1}$) as seen in Figure S5, Supporting Information.^[43]

2.1.2. Folate-Modified GOX-NR (F-GOX@NR)

To enable folate receptor targeting of nanoreactors, we prepared a folate-modified GOX@NR (F-GOX@NR) by reacting succinimidyl-PEG₃₄₀₀-folate with the amino groups on the surface of the GOX@NR (Figure 1c). As the folate receptor is upregulated on many types of cancer cells over normal cells, the specific binding and uptake into folate-receptor positive cancer cells were expected by folate-functionalized nanoparticles.^[47–50] The number of folate groups on the nanoreactors was estimated to be ca. 700 ± 120 by measuring the amount of unreacted folate from the supernatant (see Supporting Information). The surface of F-GOX@NR was further modified by succinimidyl-methoxy-PEG₂₀₀₀ to prevent non-specific uptake by cells. Upon the modification of the GOX@NR, the enzymatic activity remained unchanged (Figure S6, Supporting Information). After modification of GOX@NR by methoxy-PEG₂₀₀₀ (control for non-targeted GOX@NR) or both methoxy-PEG₂₀₀₀ and succinimidyl-PEG₃₄₀₀-folate (F-GOX@NR), the hydrodynamic

diameter slightly increased, which is a typical characteristic of PEGylated nanoparticles by the formation of PEG layers on the surfaces.

2.1.3. Stability of GOX in Nanoreactors

The stability of GOX was investigated by nano differential scanning fluorimetry (NanoDSF). Thermal denaturation profiles revealed an increased melting temperature (T_m) of GOX in the nanoreactors (T_m : 76 °C), in contrast to native GOX (T_m : 64 °C) and GOX (T_m : 68 °C) attached on the surface of silica nanoparticles (Figure 1d). The increased T_m indicated enhanced stability of GOX after encapsulation into the nanoreactor, which might allow longer half-lives at physiological temperature. At 37 °C, the native GOX gradually loses its enzymatic activity, reaching only 10% after 30 min.^[51] The higher stability can be explained by enhanced refolding of the immobilized enzymes as reported previously.^[45] GOX inside of the nanoreactors is bound to the silica matrix by multiple attachments points, which we believe explains the high stability, even higher than surface-immobilized GOX.

The enzymatic activity of GOX and GOX@NR in cell lysates from three different cell lines was investigated (MDA-MB-231, MCF-7, and Caco-2, 5.0×10^6 cells mL⁻¹). These cell lines were also used for the further cytotoxicity assays. After 72 h, native GOX lost its enzymatic activity to ≈75–80% of the initial activity, while the activity of GOX@NR remained unchanged (Figure 1e). Since there are many proteolytic factors in the intracellular environment, the protection of enzymes encapsulated into silica nanoreactors is one of the crucial factors for future in vivo studies. Also, using proteinase-K, GOX@NR kept its enzymatic activity (Figure S7, Supporting Information, additional discussion section in Supporting Information).

2.2. Design of COX-2 Targeted and ROS-Cleavable Prodrug (5)

2.2.1. Synthesis of Celecoxib/SN-38 Prodrug (5)

To develop an ROS-cleavable prodrug, we introduced a thioketal linker as a ROS-responsive unit^[21,52–56] between celecoxib as a COX-2 targeting moiety and 7-ethyl-10-hydroxyl-camptothecin (SN-38) as a topoisomerase I inhibitor (Figure 2a).^[39,40] Celecoxib is an antagonist with high selectivity and affinity (K_d : 2.3 nM) toward COX-2 not COX-1.^[57] 5 is expected to selectively respond to COX-2 overexpressed cells,^[58] providing an anti-inflammatory effect via COX-2 inhibition.^[23] Upon the cleavage of the thioketal by abundant ROS in tumors, 5 is activated to release SN-38, allowing selective and efficient tumor death.

The synthesis of 5 is outlined in the Experimental Section and summarized in Scheme S1, page 12 in Supporting Information. The thioketal linker was prepared by previously reported procedures,^[59] starting from Cel-Cl, followed by EDC coupling with the carboxylic acid group of celecoxib scaffold. Intermediate 4 was activated by triphosgene and treated with SN-38 to afford 5. All intermediates, reference compounds, and the final product were confirmed by standard analytical techniques such as ¹H NMR, ¹³C NMR, and ESI-MS (Figures S8–S19, Supporting Information).

2.2.2. ROS-Triggered Cleavage of Prodrug

We investigated the H₂O₂-mediated thioketal linker cleavage in 5 by fluorescence spectroscopy. 5 showed a fluorescence band at 452 nm originated from SN-38 with a bathochromic shift to ca. 560 nm upon the thioketal cleavage by H₂O₂. The bathochromic shift can be attributed to an ICT (intramolecular charge transfer), which is more developed in SN-38 than in 5 (Figure 2b; Figure S20, Supporting Information).^[60] 5 (5.0 μM in phosphate-buffered saline) was incubated with various concentrations of H₂O₂ (1, 10, 30, and 50 mM) and with different incubation times, proving a higher release of SN-38 with increasing H₂O₂ concentration and longer incubation times (Figure 2c,d). The thioketal linker can also be cleaved by hydroxyl radicals (·OH),^[21,52–56] which is important because the hydroxyl radicals can be generated in cancer cells by a Fenton-like reaction in the presence of H₂O₂. The fluorescence intensity at 560 nm of 5 was enhanced in the presence of ·OH (Figure S21, Supporting Information), indicating the release of SN-38 and confirming that the 5 can be activated by ROS (H₂O₂ and hydroxyl radicals).

HPLC analysis was conducted to prove the mechanism of prodrug activation by H₂O₂ (Figure 2e). After the incubation of 5 with H₂O₂ for different times (0, 1, 12, 24, and 48 h), HPLC analysis was performed. To assign the newly formed signals, we utilized two wavelengths, that is, 254 and 365 nm, to detect the two cleaved units, as they have different UV-absorption spectra (Figure S22, Supporting Information). While the peak of 5 was detected at 34.1 min when incubated for 1 h, new signals were detected at 5.3 and 36.3 min when monitored at 254 nm, resulting from the instant cleavage of the thioketal (Figure S22, Supporting Information, left). Owing to the fact that celecoxib-derivatives have strong absorbance at 254 nm rather than 365 nm, the peak at 5.3 min was assigned to the formed celecoxib-conjugated parts, whereas SN-38-derivatives proved a significant signal at ca. 36.3 min. Considering that the cleaved SN-38-conjugated units undergo the intramolecular cyclization by nucleophilic attack of the thiol group, a gradual reduction of the signals from SN-38 conjugated molecules at 36.3 min was observed for longer incubation times, while the signal at 6.3 min, which was assigned to free SN-38, simultaneously increased.^[56] Furthermore, we calculated the ratio of absorbance at 6.3 min and 36.3 min ($A_{6.27}/A_{36.39}$) to underline the kinetics of the drug activation, indicating a gradual increase of the ratio (Figure S23, Supporting Information). Further, HPLC was used to quantify the amounts of activated drug after the treatment of H₂O₂. The ratio of absorbance (A/A_0) was calculated, where A is the value of absorbance at different intervals (1, 12, 24, and 48 h) and A_0 is the one of 50 μM of SN-38. As expected, the concentration of activated drug increased over time with ≈44.7% of released SN-38 after 48 h under these conditions (Figure S24, Supporting Information).

2.3. Evaluation of F-GOX@NR-Mediated Cancer Cell Death

2.3.1. Cytotoxicity of F-GOX@NR by Folate Receptor Targeting and Enzymatic Reactions

We evaluated the cellular targeting and cytotoxicity of F-GOX@NR to MCF-7 cancer cells carrying folate receptors allowing

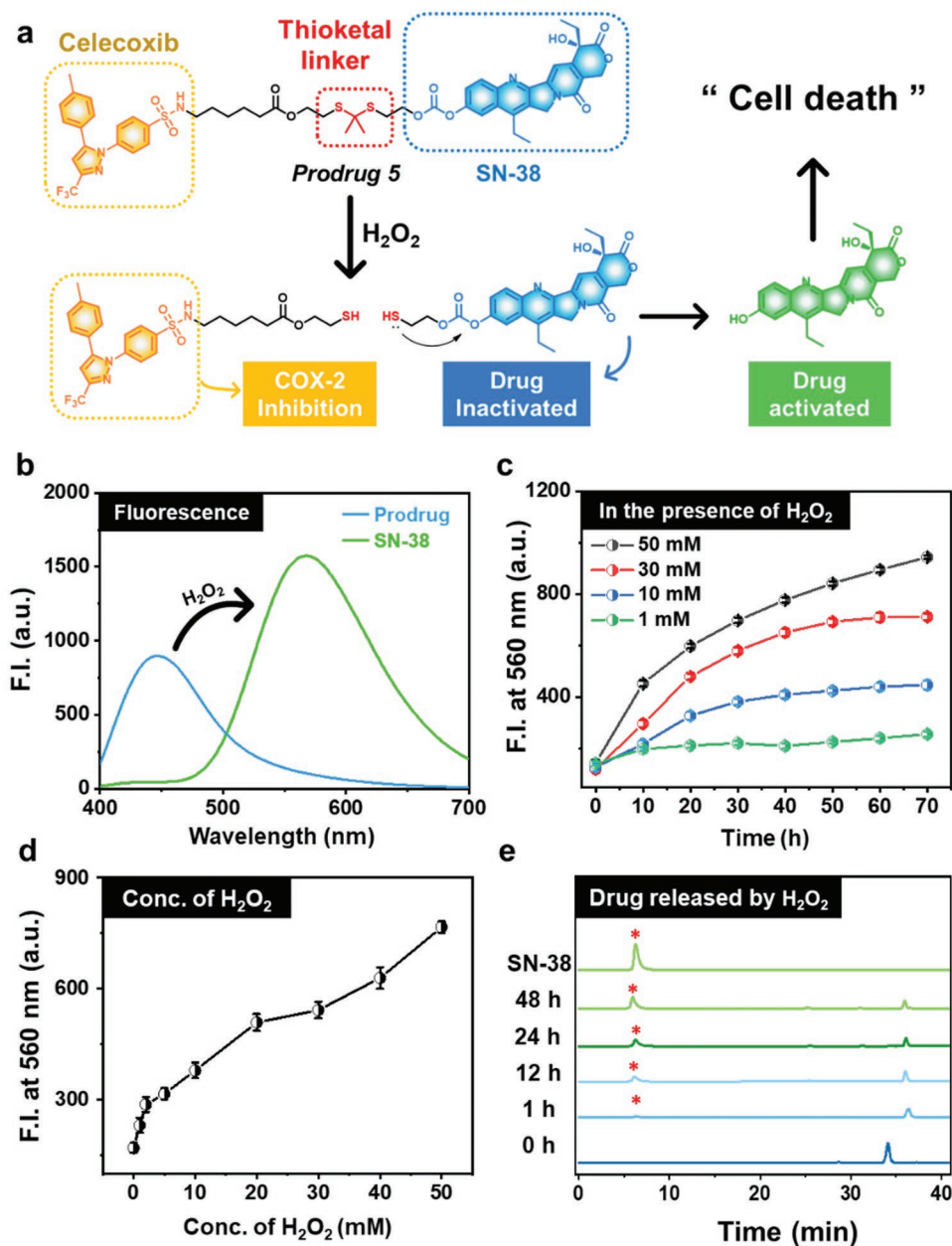


Figure 2. Cleavage of the prodrug (5) by H₂O₂. a) Proposed activation mechanism of 5 in the presence of H₂O₂. b) Fluorescence of 5 (5.0 μM) and SN-38 in PBS buffer (37 °C, pH = 7.4). c) Fluorescence intensity changes of 5 (5.0 μM) at 560 nm upon incubation with different concentrations of H₂O₂ (1, 10, 30, and 50 mM) for 70 h in PBS buffer (37 °C, pH = 7.4). d) Fluorescence changes of 5 (5.0 μM) in various concentrations of H₂O₂ for 72 h in PBS buffer. e) HPLC analysis for activation of 5. All peaks were observed from incubation of 5 (50 μM) in the presence of H₂O₂ (50 mM) at different times (0 h (only 5), 1 h, 12 h, 24 h, and 48 h). Newly formed peaks (asterisk) corresponding to SN-38 were denoted (measured at 365 nm).

F-GOX@NR to be delivered into the cells through a folate receptor-mediated endocytosis.^[47–50] After uptake into the cells, the semipermeable nanoreactors allow the GOX reaction with substrates (glucose and O₂) to produce H₂O₂ and gluconic acid inside the cells (Figure 3a). As both glucose and O₂ are essential in living organisms, the H₂O₂-production by GOX in the cells is expected to lead to efficient cytotoxicity.

Prior to the cell death assay of F-GOX@NR, the toxicity of empty silica nanoreactors was investigated as a control. When cells were incubated with empty silica nanoparticles (without

GOX) for 5 h, they did not show significant cytotoxicity up to 200 μg mL⁻¹ (Figure S25, Supporting Information). For the cell tests with F-GOX@NR, we stayed below this threshold and used 20 μg mL⁻¹ for the next in vitro cell studies. The cytotoxicity level is in accordance with a previous report that describes lower toxicity of 40 – 80 nm (∅) sized silica nanoparticle than larger nanoparticles.^[61]

We investigated the binding and uptake of the F-GOX@NR to the folate receptor-positive MCF-7 cells by confocal microscopy (Figure 3b). Fluorescein-labeled F-GOX@NRs

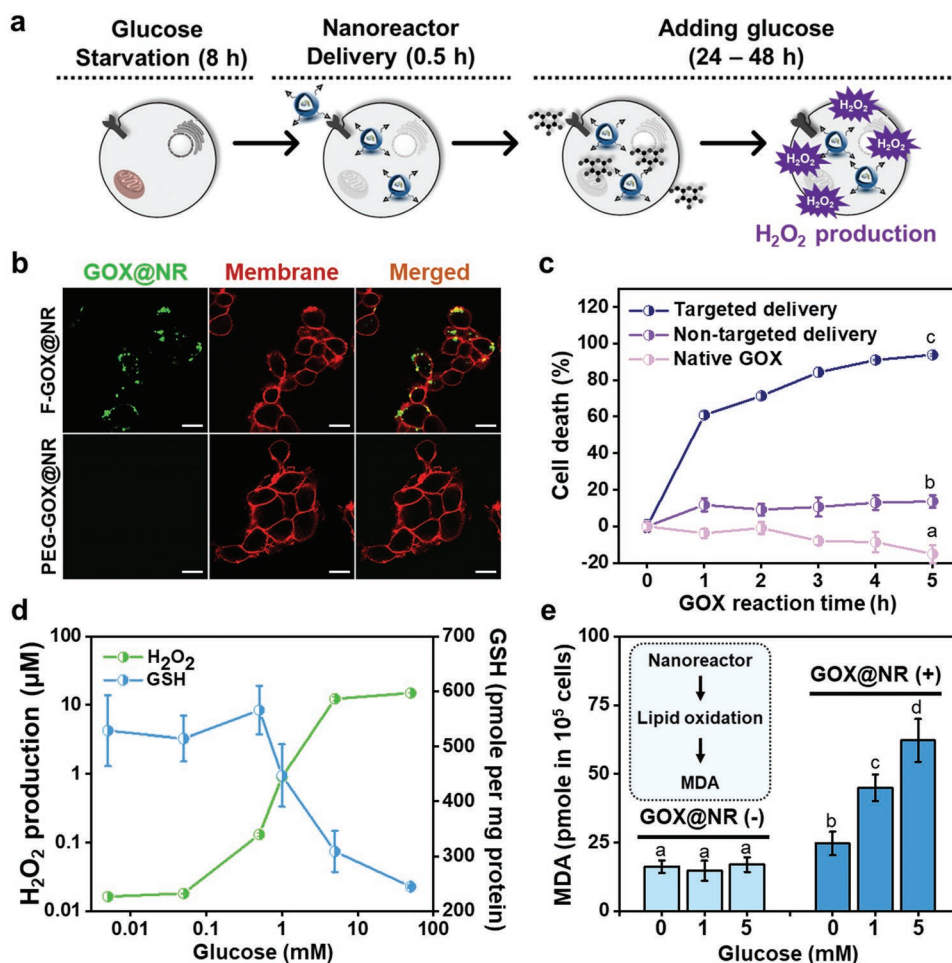


Figure 3. Folate receptor-targeted delivery of F-GOX@NR into MCF-7 cells. a) Schematic illustration for folate receptor-targeted endocytosis of F-GOX@NR and H₂O₂-induced cytotoxicity. b) Delivery of F-GOX@NR into MCF-7 cells. c) Cytotoxicity of F-GOX@NR to MCF-7 cells (30 min delivery and 50 mM glucose). Targeted delivery indicates the use of F-GOX@NR, and non-targeted delivery indicates the use of PEGylated GOX@NR. d) Determination of H₂O₂-production (green) and glutathione (GSH)-reduction (blue) in F-GOX@NR treated MCF-7 cells upon 30 min delivery and 2.5 h glucose reactions. e) Lipid peroxidation assay by treatment of F-GOX@NR under glucose dose-responses in MCF-7 cells. Increasing production of MDA (malondialdehyde) indicates increased oxidation of unsaturated lipids. Data are represented as mean ± SEM (*n* = 3 in (c) and (e)). Statistical significance was determined by a one-way ANOVA test with a post-hoc Bonferroni test. Different letters (e.g., a–d) signify datasets that are statistically distinct (*p* < 0.05).

were incubated with the cells for 30 min. After that we observed a significant fluorescence indicative for binding and uptake of the F-GOX@NR into the cells. In addition, the flow cytometry underlined the binding of F-GOX@NR to the folate receptor-positive MCF-7 cells (Figure S26, Supporting Information). In contrast, for the non-targeted GOX@NR, only a negligible uptake of nanoparticles into the cells was detected. The uptake of F-GOX@NR into the MCF-7 cells was quantified: when we incubated 2 µg (in 100 µL) of the fluorescein-labeled F-GOX@NR with the cells for 30 min, we calculated the uptake amount of 0.18 ± 0.02 µg, that is, 9% uptake efficiency, which corresponds to $\approx 4100 \pm 4000$ nanoreactors (12 ± 1 pg) were delivered into each single cell (note: the weight of single-cell ≈ 2.3 ng)^[62] calculations in the Supporting Information). After 90 min of incubation the uptake efficiency of F-GOX@NR increased to $\approx 14\%$ (Figure S27, Supporting Information).

The cytotoxicity of F-GOX@NR were investigated in different concentrations of glucose (0–50 mM). To prevent the

GOX reaction and undesired cell death before intracellular delivery of F-GOX@NR, the cells were first incubated under glucose-free conditions for 8 h. The “starving” period did not have negative impacts on the cell viability and only 8% less proliferation of the cells was observed in comparison to cells that were incubated with serum-free conditions. After glucose starvation of the cells, we delivered the nanoreactors to the cells for 30 min, washed out the undelivered nanoreactors, then further incubated with glucose-containing condition for 5 h. F-GOX@NR resulted in high cytotoxicity, while non-functionalized nanoreactors and native GOX revealed no significant toxicity under these conditions, due to very low cellular uptake (Figure 3b,c; Figure S28, Supporting Information). In a separate experiment, we studied competitive binding of F-GOX@NR, when additional folate (250 µM) was added to the cells (Figure S29, Supporting Information): a decreased cytotoxicity compared to the experiment without additional folate was detected, which further supports the folate receptor-mediated delivery of F-GOX@NR.

The cytotoxicity of the folate receptor-targeting system was evaluated in different cancer cell lines at various glucose concentrations. MCF-7 (breast cancer) and Caco-2 cells (colorectal cancer) are folate receptor-positive cells, while we selected MDA-MB-231 (breast cancer) as a folate receptor-negative cell as control (folate receptor expression: Figure S30, Supporting Information). F-GOX@NR effectively led to the cell death of both folate receptor-positive cells (for MCF-7 >1 mM glucose and for Caco-2 cells >5 mM glucose, Figure S31, Supporting Information). Notably, we achieved significant cytotoxicity in the range of physiological glucose conditions (5 mM). Additionally, only a low cellular uptake of F-GOX@NR into the folate receptor-negative cells (MDA-MB-231) was observed, followed by negligible cell death was observed at all glucose concentrations (cf. flow cytometry data Figure S32, Supporting Information).

2.3.2. Oxidative Stress of Cancer Cells by F-GOX@NR

To further understand the connection between the glucose concentration and the amount of available H₂O₂ that might lead to cytotoxicity or cleavage of the prodrug, we applied a H₂O₂-responsive fluorescent probe. Notably, the H₂O₂ production increased in a nonlinear correlation with the glucose concentration, which explains the very low viability of MCF-7 cells at high glucose concentrations (Figure 3d, green curve). It appears that concentrations above 200 nM are critical for the H₂O₂-induced cell death; the H₂O₂-level of non-treated cells was found to be ca. 20 nM. The amount of glutathione was determined by the Ellman assay. As Ellman reagent (5,5'-dithiobis-(2-nitrobenzoic acid) is only reactive to the reduced form of GSH, the remaining capacity of anti-oxidative defense can be estimated. The GSH level decreased gradually with increasing amounts of glucose (Figure 3d, blue curve), indicating the crucial contribution to oxidative damages inside of cells. Another important mechanism in oxidative cell death is lipid peroxidation, which disrupts the cell membrane.^[63] The malondialdehyde (MDA) assay is a good indicator to determine the peroxidation of unsaturated phospholipids.^[64] MCF-7 cells were treated with F-GOX@NR to MCF-7 in the presence of glucose (0, 1, and 5 mM, respectively) for 3 h and then, the degree of peroxidation by MDA assay using cell lysate was determined. At glucose concentrations of 1 and 5 mM, the degree of peroxidation increased by a factor of 2.5 and 3 compared to the cells without glucose and the nanoreactors, respectively (Figure 3e). In contrast, no significant changes in the degree of peroxidation were observed without F-GOX@NR or glucose. It is known that the peroxidation of phospholipids increases cell membrane rigidity, which occurs an unexpected impact on permeability and behaviors of membrane-bound proteins, thereby leading to cell death.^[65]

2.4. Evaluation of Prodrug (5)-Mediated Cancer Cell Death

2.4.1. Intracellular COX-2 Targeting of Celecoxib and Prodrug

We investigated the intracellular COX-2 targeting ability of celecoxib (Figure 4a) toward MCF-7 cells, which express COX-2. Since 5 is not strongly fluorescent, we synthesized a

fluorophore (rhodamine)-labeled celecoxib (Rho-Cel) instead (Scheme S2 and Figure S33, Supporting Information). On fixed cells, we observed the co-localization of celecoxib (rhodamine) and anti-COX-2 antibodies (FITC-labeled) in the cytoplasm by confocal laser microscopy (Figure 4b), confirming that the celecoxib unit of the Rho-Cel successfully targeted COX-2 in the cells.^[66] It is a critical sign that the celecoxib-decorated molecules might be accumulated in cytoplasm by specific binding to the intracellular COX-2, allowing the exclusive activation inside the cells.

Additionally, we evaluated the secretion of PGE₂ for confirming anti-inflammatory response in MCF-7, whether a celecoxib-modified 5 inhibits COX-2. The decreased secretion of PGE₂ was observed in the MCF-7 cells pretreated with 5 or celecoxib (Figure 4c), indicating successful binding of 5 to COX-2. In contrast, no inhibitory effect of COX-2 was seen with only SN-38.

2.4.2. Cytotoxicity of Prodrug

Cytotoxicity of the 5 against MCF-7 (COX-2 positive) and Caco-2 (COX-2 negative) revealed a higher effect on MCF-7 (IC₅₀: 0.43 μM) than on Caco-2 (IC₅₀: 17.6 μM), resulting from the COX-2 guiding effect by the prodrug conjugated with a celecoxib unit (Figure S34, Supporting Information; Figure 4d). Thus, the 5 could target COX-2 and exhibit outstanding therapeutic effects by H₂O₂-responsive drug activation and COX-2 inhibitory effect in COX-2 positive cells. For such cytotoxicity, SN-38 is a high potency anti-neoplastic drug by inhibiting topoisomerase in the cells,^[39,40] which gives a key contribution to obtain the submicromolar level in IC₅₀ to this experiment. As prodrug form of SN-38 (5) is not highly active, only after cleavage of the thioketal linker by H₂O₂ a significant cytotoxicity was observed.

2.5. Synergistic Cell Death by Dual-Targeting of F-GOX@NR and 5

With these promising results on F-GOX@NR and the 5 separately, we investigated the dual-targeting to identify possible synergistic effects (Scheme 1). With our three cell lines different scenarios can be investigated: the MCF-7 cells function as positive control carrying both folate receptor and COX-2; Caco-2 carries only folate receptors but no COX-2; and MDA-MB-231 cells are COX-2-positive but folate-negative cells. As F-GOX@NR led to the high degree of cell death (>90%) at 5 mM glucose conditions regardless of COX-2 expression levels (Figure 3c; Figure S28, Supporting Information), we used a 1 mM glucose condition in this assay. About low glucose levels, some deep tumor environments show low glucose and oxygen condition due to limited supplying the nutrients and reprogrammed metabolism.^[67,68] We set the experimental conditions that led to ca 50% cell death (IC₅₀) by each F-GOX@NR (4 μg mL⁻¹) or SN-38 (100% activated form) (Figure S35, Supporting Information), respectively. The cytotoxicity assay showed that ca. 90% cell death for MCF-7 was achieved by the co-treatment of F-GOX@NR and 5 (Figure 5b). In contrast,

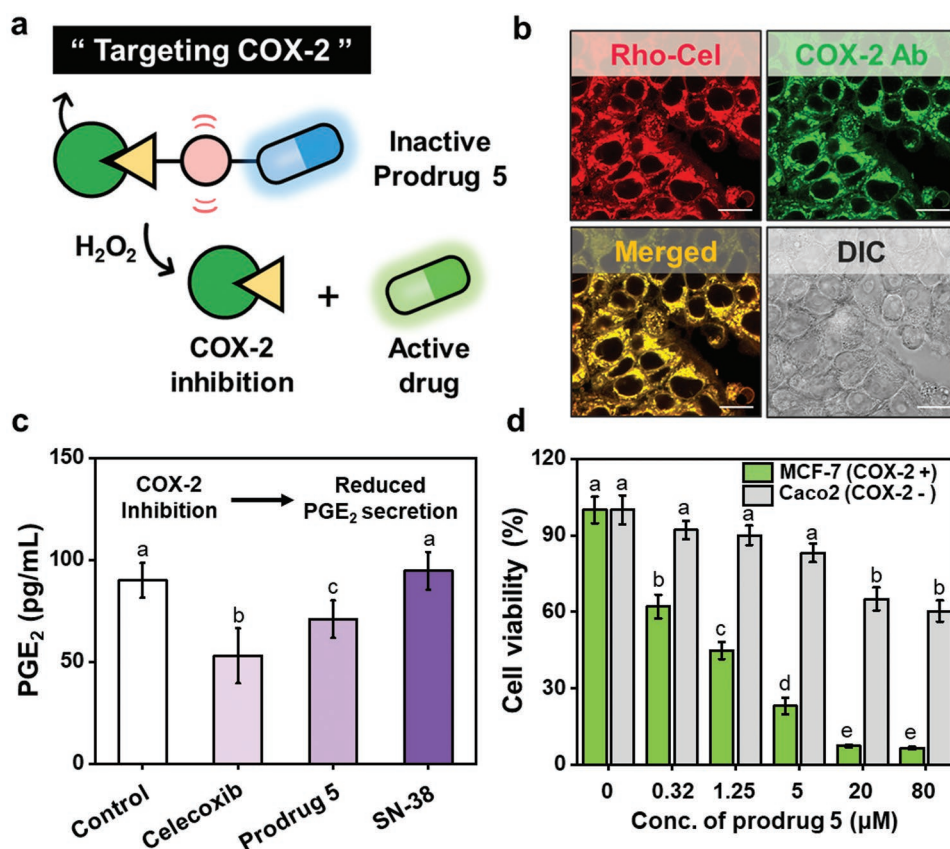


Figure 4. Cytotoxicity of the COX-2 targeted celecoxib/SN-38 prodrug (5). a) Cleavage of thioketal linker by H₂O₂ activates the 5. b) Co-localization imaging of the fluorescence signal from 10 μM Rho-Cel (ex 570 nm/em 580–620 nm; red color), anti-COX-2 antibody (ex 488 nm/em 500–540 nm; green color), and merged image (yellow) in MCF-7 cells (×100 magnification). Scale bar = 15 μm. c) Changes in PGE₂ secretion in MCF-7 by treatment of 5, celecoxib or SN-38. d) Cell viability of COX-2 positive cell (MCF-7) and COX-2 negative cell (Caco-2) by 5 for 48 h incubation at 5 mM glucose. Data are represented as mean ± SEM (*n* = 3 in (c) and (d)). Statistical significance was determined by a two-way ANOVA test with a post-hoc Bonferroni test. Different letters (e.g., a–e) signify datasets that are statistically distinct (*p* < 0.05).

the same cocktail resulted to a lower cytotoxicity in Caco-2 cells (60%) as only F-GOX@NR is effective. Similarly, MDA-MB-231 revealed 50% residual viability as only 5 induced cytotoxicity. These results suggested that the use of both F-GOX@NR and 5 selectively induce the death of the dual-positive cells (MCF-7), thus indicating more specific anticancer strategy rather than single-targeting approaches. F-GOX@NR and 5 can be accumulated together inside the same cell, which have more opportunities to be efficiently activated by produced H₂O₂.

The amount of produced H₂O₂ by F-GOX@NR was measured for a period of 24 h. The F-GOX@NR-treated cells gave 14 μmol of H₂O₂ after 24 h, enough to activate 5 (1.0 nmol; 10 μM, Figure S36, Supporting Information). Non-treated cells produced only 0.8 μmol of intrinsic H₂O₂ after 24 h. The higher H₂O₂ concentration enabled the more efficient activation of 5 (Figure 2a,d). When the concentration of glucose or 5 were varied, the degree of cytotoxicity could be adjusted. Below 1.0 mM glucose, the F-GOX@NR led to 40% cell death in 24 h and 55% in 48 h. When both F-GOX@NR and 5 were administered to MCF-7, an increased cytotoxicity was detected (right panel in Figure 5c and Figure S37, Supporting Information) compared to 5 alone (left panel in same figures). By

dosing of 5 (2.0 μM) and F-GOX@NR (0.4 μg mL⁻¹), a cytotoxicity of ≈90% was observed. This value for the cytotoxicity was ca. 20% higher compared to the sum of the two separate treatments (Figure S38, Supporting Information), which would have resulted in 70% cell death (i.e., 40% by F-GOX@NR and 30% by 5). The additional cytotoxicity of the mixture implies a clue of synergistic effect by combining F-GOX@NR and 5.

For further investigation of the synergistic effects, we evaluated the IC₅₀ value of each drug and a combination of F-GOX@NR and 5 after 24 h and 48 h incubation (Figure 5d). As SN-38 is a well-known antineoplastic drug, a high potency was observed with IC₅₀ = 1.2 μM (for 24 h) and 0.54 μM (for 48 h). 5 showed a higher IC₅₀ = 3.8 μM (for 24 h) as it needs activation by intrinsic H₂O₂ in cells. The potency of 5 in 48 h was not significantly different (IC₅₀: 2.8 μM in 48 h) possibly due to lack of intrinsic H₂O₂ by death of cells. Interestingly, when 5 was combined with F-GOX@NR (4 μg mL⁻¹ for 24 h, and 2 μg mL⁻¹ for 48 h), a remarkably high potency of 5 (IC₅₀: 0.14 μM in 24 h, and 0.1 μM in 48 h) was observed. To underline that such the high potency is not an additive effect but a real synergy, we plotted the IC₅₀ values in a so-called isobologram (Figure S39, Supporting Information).^[69,70] The calculated combination index of 0.78 also supports the synergistic

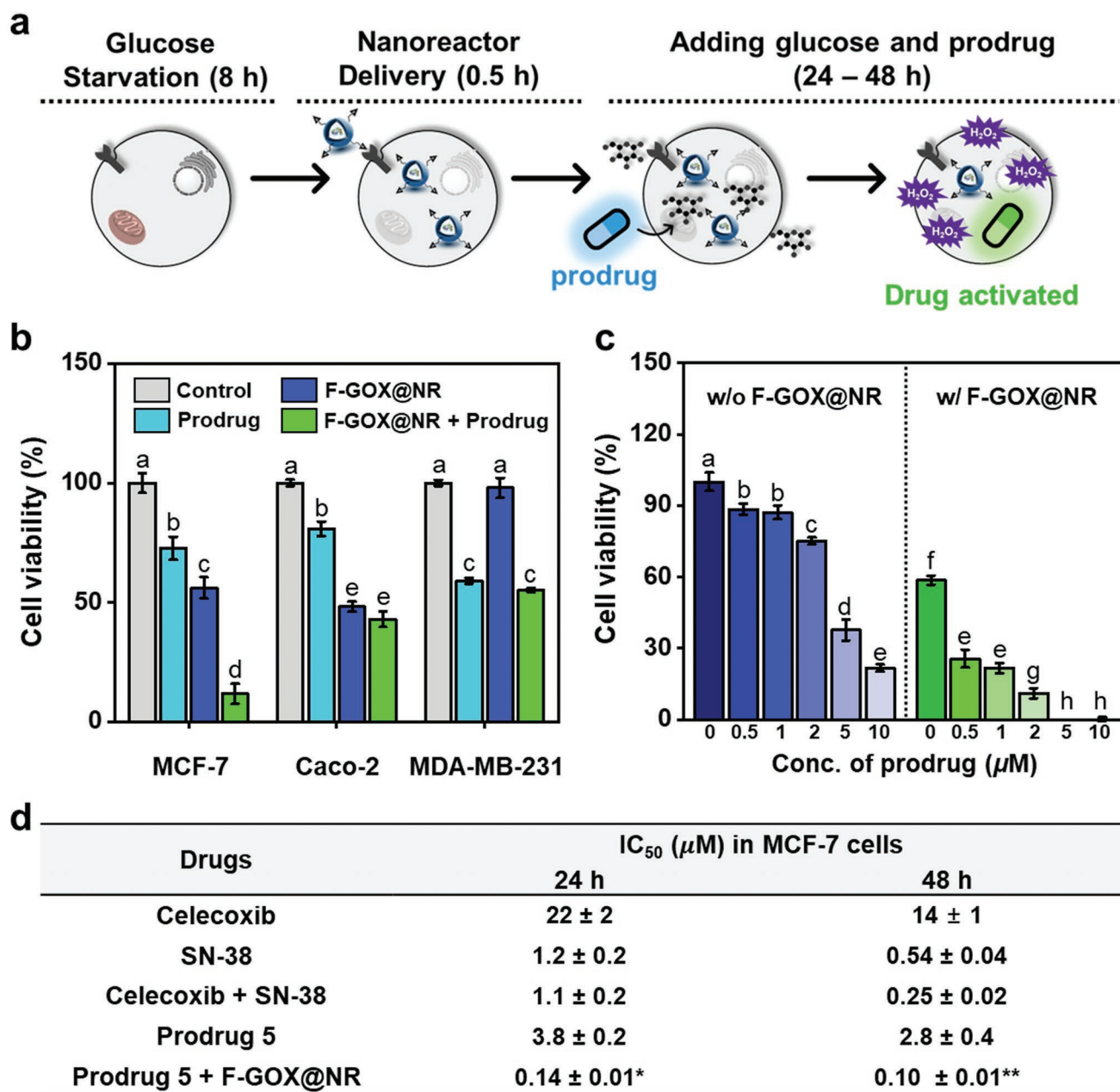


Figure 5. Dual-targeting of F-GOX@NR and celecoxib/SN-38 prodrug (5) for synergistic cytotoxicity. a) Schematic illustration for dual-targeting strategy by F-GOX@NR and 5. After a glucose starving-period (8 h), the cells are incubated with F-GOX@NR for 30 min, the non-uptake F-GOX@NR removed, then 5 is added and incubated for 24 or 48 h. b) Cell viability of different cell lines after with treatment with F-GOX@NR and 5 (MCF-7 (folate receptor +; COX-2 +), Caco-2 (folate receptor +; COX-2 -), MDA-MB-231 (folate receptor -; COX-2 +)). Glucose (1.0 mM) was added, and GOX reaction was conducted for 24 h. c) Cell viability by 5 only, F-GOX@NR only, and co-treatment of 5 and F-GOX@NR with the treatment of 1.0 mM glucose and GOX reaction for 24 h in MCF-7. d) IC₅₀ of drugs with 1.0 mM glucose at 24 h and 48 h in MCF-7 cells. Data are represented as mean ± SEM ($n = 3$ in (b) and (c)). *F-GOX@NR of 4 μg mL⁻¹ was used for the assay. **F-GOX@NR of 2 μg mL⁻¹ was used for the assay. Statistical significance was determined by a two-way ANOVA test with a post-hoc Bonferroni test. Different letters (e.g., a–h) signify datasets that are statistically distinct ($p < 0.05$).

effect of the combination of F-GOX@NR and 5 (for details regarding the isobologram and the combination index, see the Supporting information). In case of 48 h incubation, the potency of 5 showed a lower potency compared to sole SN-38 or combination of SN-38 and Celecoxib, however, synergistic effects of F-GOX@NR and 5 were also observed. Therefore, one of the advantages of the combination in F-GOX@NR and

5 is requirement of the shorter time and the less amount of prodrugs to obtain the higher potency compared to drug only. The synergism in the combination of F-GOX@NR and 5 might be caused by i) enhanced 5 uptake as the cell membrane was oxidized, ii) more efficient activation of 5 by F-GOX@NR, and iii) decreased defense metabolism of cells under glucose-depleted conditions.

3. Conclusions

In summary, we developed a novel anticancer strategy exerting a synergistic effect by the dual-targeted H₂O₂-generating nano-reactors and a ROS-activated prodrug. We successfully prepared GOX-loaded silica nanoparticles (F-GOX@NR) functionalized with folate groups as a semipermeable nanoreactor to specifically target cancer cells and to produce hydrogen peroxide from glucose intracellularly. A novel prodrug (5) bearing celecoxib and SN-38 anticancer agents conjugated with an H₂O₂-cleavable thioketal linker was designed. The 5 can bind to the intracellular COX-2-receptor in cancer cells, allowing longer retention time in the cytoplasm and was readily activated by H₂O₂ produced from F-GOX@NR to deliver the SN-38 anticancer drug inducing cell apoptosis. For dual-positive cancer cells with the folate receptors and COX-2, we demonstrated a synergistic cytotoxicity by F-GOX@NR and the Celecoxib-conjugated 5. We suggest that our dual-targeting and synergistic strategy might pave the way for an effective and tailored anticancer strategy.

Supporting Information

Supporting Information is available from the Wiley Online Library or from the author.

Acknowledgements

S.-M.J. and H.S.K. contributed equally to this work. This work was part of the MaxSynBio consortium, jointly funded by the Federal Ministry of Education and Research of Germany and the Max Planck Society. This work was supported by the National Research Foundation of Korea (NRF) funded by the Ministry of Science and ICT (CRI Project No. 2018R1A3B1052702 and 2019M3E5D1A01068998, J.S.K.), Basic Science Research Program (2020R1A6A3A01100551, M.W.) funded by the Ministry of Education. The authors sincerely thank Dr. Robert Graf (MPIP) for solid-state NMR spectroscopy studies. The authors thank Ute Heinz (MPIP) and Petra Räder (MPIP) for analytical support.

Open access funding enabled and organized by Projekt DEAL.

Conflict of Interest

The authors declare no conflict of interest.

Data Availability Statement

The data that support the findings of this study are available in the supplementary material of this article.

Keywords

chemodynamic therapeutics, dual-targeting, nanoreactors, ROS-responsive prodrugs, synergistic cancer therapy

Received: January 20, 2022

Revised: February 27, 2022

Published online:

- [1] J. Li, Z. Wei, X. Lin, D. Zheng, M. Wu, X. Liu, J. Liu, *Adv. Healthcare Mater.* **2019**, *8*, 1801627.
- [2] H. Cheng, X.-Y. Jiang, R.-R. Zheng, S.-J. Zuo, L.-P. Zhao, G.-L. Fan, B.-R. Xie, X.-Y. Yu, S.-Y. Li, X.-Z. Zhang, *Biomaterials* **2019**, *195*, 75.
- [3] J. F. Mukerabigwi, W. Yin, Z. Zha, W. Ke, Y. Wang, W. Chen, A. A.-W. M. M. Japir, Y. Wang, Z. Ge, *J. Controlled Release* **2019**, *303*, 209.
- [4] Z. Yu, P. Zhou, W. Pan, N. Li, B. Tang, *Nat. Commun.* **2018**, *9*, 5044.
- [5] D. R. Liston, M. Davis, *Clin. Cancer Res.* **2017**, *23*, 3489.
- [6] Y. Zorkina, O. Abramova, V. Ushakova, A. Morozova, E. Zubkov, M. Valikhov, P. Melnikov, A. Majouga, V. Chekhonin, *Molecules* **2020**, *25*, 5294.
- [7] R. Mahfoozur, S. Gajanand, T. Kanika, A. Firoz, O. P. Katara, G. G. Vijay, K. Vikas, A. Z. Mazin, A. Sohail, *Curr. Top. Med. Chem.* **2017**, *17*, 162.
- [8] T. Khan, M. Mayuresh Patkar, M. Momin, A. Omri, *Expert Opin. Drug Delivery* **2020**, *17*, 903.
- [9] X. Lian, Y. Huang, Y. Zhu, Y. Fang, R. Zhao, E. Joseph, J. Li, J.-P. Pellois, H.-C. Zhou, *Angew. Chem., Int. Ed.* **2018**, *57*, 5725.
- [10] L.-H. Fu, C. Qi, Y.-R. Hu, J. Lin, P. Huang, *Adv. Mater.* **2019**, *31*, 1808325.
- [11] C. Wang, J. Yang, C. Dong, S. Shi, *Adv. Ther.* **2020**, *3*, 2000110.
- [12] M. Wang, D. Wang, Q. Chen, C. Li, Z. Li, J. Lin, *Small* **2019**, *15*, 1903895.
- [13] S.-M. Jo, F. R. Wurm, K. Landfester, *Nano Lett.* **2020**, *20*, 526.
- [14] Y. Ma, Y. Zhao, N. K. Bejjanki, X. Tang, W. Jiang, J. Dou, M. I. Khan, Q. Wang, J. Xia, H. Liu, Y.-Z. You, G. Zhang, Y. Wang, J. Wang, *ACS Nano* **2019**, *13*, 8890.
- [15] W. Fan, N. Lu, P. Huang, Y. Liu, Z. Yang, S. Wang, G. Yu, Y. Liu, J. Hu, Q. He, J. Qu, T. Wang, X. Chen, *Angew. Chem., Int. Ed.* **2017**, *56*, 1229.
- [16] L. Mei, D. Ma, Q. Gao, X. Zhang, W. Fu, X. Dong, G. Xing, W. Yin, Z. Gu, Y. Zhao, *Mater. Horiz.* **2020**, *7*, 1834.
- [17] J. Li, Y. Li, Y. Wang, W. Ke, W. Chen, W. Wang, Z. Ge, *Nano Lett.* **2017**, *17*, 6983.
- [18] R. Zhang, L. Feng, Z. Dong, L. Wang, C. Liang, J. Chen, Q. Ma, R. Zhang, Q. Chen, Y. Wang, Z. Liu, *Biomaterials* **2018**, *162*, 123.
- [19] Y. Guo, H.-R. Jia, X. Zhang, X. Zhang, Q. Sun, S.-Z. Wang, J. Zhao, F.-G. Wu, *Small* **2020**, *16*, 2000897.
- [20] S. Dinda, S. Sarkar, P. K. Das, *Chem. Commun.* **2018**, *54*, 9929.
- [21] W. Zhang, X. Hu, Q. Shen, D. Xing, *Nat. Commun.* **2019**, *10*, 1704.
- [22] J. Xia, Q. Pei, M. Zheng, Z. Xie, J. Mater. Chem. B **2021**, *9*, 2308.
- [23] A. Sharma, M.-G. Lee, M. Won, S. Koo, J. F. Arambula, J. L. Sessler, S.-G. Chi, J. S. Kim, *J. Am. Chem. Soc.* **2019**, *141*, 15611.
- [24] M. Won, S. Koo, H. Li, J. L. Sessler, J. Y. Lee, A. Sharma, J. S. Kim, *Angew. Chem., Int. Ed.* **2021**, *60*, 3196.
- [25] A. Sharma, J. Chun, M. S. Ji, S. Lee, C. Kang, J. S. Kim, *ACS Appl. Bio Mater.* **2021**, *4*, 2026.
- [26] O. Tietz, J. Kaur, A. Bhardwaj, F. R. Wuest, *Org. Biomol. Chem.* **2016**, *14*, 7250.
- [27] A. Bhardwaj, J. Kaur, F. Wuest, E. E. Knaus, *ChemMedChem* **2014**, *9*, 109.
- [28] H. S. Kim, A. Sharma, W. X. Ren, J. Han, J. S. Kim, *Biomaterials* **2018**, *185*, 63.
- [29] M. Fernández, F. Javaid, V. Chudasama, *Chem. Sci.* **2018**, *9*, 790.
- [30] I. G. Campbell, T. A. Jones, W. D. Foulkes, J. Trowsdale, *Cancer Res.* **1991**, *51*, 5329.
- [31] J. A. Ledermann, S. Canevari, T. Thigpen, *Ann. Oncol.* **2015**, *26*, 2034.
- [32] H. Wang, L. Cheng, S. Ma, L. Ding, W. Zhang, Z. Xu, D. Li, L. Gao, *ACS Appl. Mater. Interfaces* **2020**, *12*, 20191.
- [33] M. C. R. Symons, S. Rusakiewicz, R. C. Rees, S. I. Ahmad, *Med. Hypotheses* **2001**, *57*, 56.

- [34] A. M. DiPietrantonio, T.-c. Hsieh, J. M. Wu, *Biochem. Biophys. Res. Commun.* **1999**, 255, 477.
- [35] K. A. Ahmad, K. B. Iskandar, J. L. Hirpara, M.-V. Clement, S. Pervaiz, *Cancer Res.* **2004**, 64, 7867.
- [36] D. Upadhyay, W. Chang, K. Wei, M. Gao, G. D. Rosen, *FEBS Lett.* **2007**, 581, 248.
- [37] T. Shinji, T. Tetsuji, M. Hirotooshi, O. Eijiro, M. Takeshi, O. Yasuyoshi, *Jpn. J. Pharmacol.* **1999**, 79, 33.
- [38] E. A. Veal, A. M. Day, B. A. Morgan, *Mol. Cell* **2007**, 26, 1.
- [39] Å. Wallin, J. Svanvik, B. Holmlund, L. Ferreud, X.-F. Sun, *Oncol. Rep.* **2008**, 19, 1493.
- [40] M. Ramesh, P. Ahlawat, N. R. Srinivas, *Biomed. Chromatogr.* **2010**, 24, 104.
- [41] Y. Yang, Y. Lu, P. L. Abbaraju, I. Azimi, C. Lei, J. Tang, M. Jambhrunkar, J. Fu, M. Zhang, Y. Liu, C. Liu, C. Yu, *Adv. Funct. Mater.* **2018**, 28, 1800706.
- [42] L. Li, Z. Yang, W. Fan, L. He, C. Cui, J. Zou, W. Tang, O. Jacobson, Z. Wang, G. Niu, S. Hu, X. Chen, *Adv. Funct. Mater.* **2020**, 30, 1907716.
- [43] S.-M. Jo, F. R. Wurm, K. Landfester, *ACS Appl. Mater. Interfaces* **2018**, 10, 34230.
- [44] S.-M. Jo, K. A. I. Zhang, F. R. Wurm, K. Landfester, *ACS Appl. Mater. Interfaces* **2020**, 12, 25625.
- [45] S.-M. Jo, F. R. Wurm, K. Landfester, *Angew. Chem., Int. Ed.* **2021**, 60, 7728.
- [46] H. Fischer, I. Polikarpov, A. F. Craievich, *Protein Sci.* **2004**, 13, 2825.
- [47] G. L. Zwicke, G. A. Mansoori, C. J. Jeffery, *Nano Rev.* **2012**, 3, 18496.
- [48] C. Deng, Q. Zhang, M. Jia, J. Zhao, X. Sun, T. Gong, Z. Zhang, *Adv. Sci.* **2019**, 6, 1801868.
- [49] M. M. Joseph, A. N. Ramya, V. M. Vijayan, J. B. Nair, B. T. Bastian, R. K. Pillai, S. T. Therakathinal, K. K. Maiti, *Small* **2020**, 16, 2003309.
- [50] D. H. Kim, D. W. Kim, J. Y. Jang, N. Lee, Y.-J. Ko, S. M. Lee, H. J. Kim, K. Na, S. U. Son, *ACS Appl. Mater. Interfaces* **2020**, 12, 37628.
- [51] N. Hashemifard, A. Mohsenifar, B. Ranjbar, A. Allameh, A. S. Lotfi, B. Etemadikia, *Anal. Chim. Acta* **2010**, 675, 181.
- [52] W. Tao, Z. He, *Asian J. Pharm. Sci.* **2018**, 13, 101.
- [53] H. Ye, Y. Zhou, X. Liu, Y. Chen, S. Duan, R. Zhu, Y. Liu, L. Yin, *Bio-macromolecules* **2019**, 20, 2441.
- [54] S. H. Lee, M. K. Gupta, J. B. Bang, H. Bae, H.-J. Sung, *Adv. Funct. Mater.* **2013**, 2, 908.
- [55] S. Shi, L. Zhang, M. Zhu, G. Wan, C. Li, J. Zhang, Y. Wang, Y. Wang, *ACS Appl. Mater. Interfaces* **2018**, 10, 29260.
- [56] Q. Pei, X. Hu, X. Zheng, S. Liu, Y. Li, X. Jing, Z. Xie, *ACS Nano* **2018**, 12, 1630.
- [57] T.-I. Natalia, D.-P. Dorota, N. B. Klaudia, C.-J. Katarzyna, M. Wojciech, *Curr. Drug Targets* **2019**, 20, 302.
- [58] H. S. Kim, T. Park, W. X. Ren, J.-Y. Lim, M. Won, J. S. Heo, S. G. Lee, J. S. Kim, *Dyes Pigm.* **2018**, 150, 261.
- [59] W. Ke, J. Li, F. Mohammed, Y. Wang, K. Tou, X. Liu, P. Wen, H. Kinoh, Y. Anraku, H. Chen, K. Kataoka, Z. Ge, *ACS Nano* **2019**, 13, 2357.
- [60] W. S. Shin, J. Han, R. Kumar, G. G. Lee, J. L. Sessler, J.-H. Kim, J. S. Kim, *Sci. Rep.* **2016**, 6, 29018.
- [61] I.-Y. Kim, E. Joachim, H. Choi, K. Kim, *Nanomedicine* **2015**, 11, 1407.
- [62] K. Park, J. Jang, D. Irimia, J. Sturgis, J. Lee, J. P. Robinson, M. Toner, R. Bashir, *Lab Chip* **2008**, 8, 1034.
- [63] A. Linden, M. Gülден, H.-J. Martin, E. Maser, H. Seibert, *Toxicol. In Vitro* **2008**, 22, 1371.
- [64] S. H. Wong, J. A. Knight, S. M. Hopfer, O. Zaharia, C. N. LeachJr., F. W. SundermanJr., *Clin. Chem.* **1987**, 33, 214.
- [65] M. Choe, C. Jackson, B. P. Yu, *F. Radic. Biol. Med.* **1995**, 18, 977.
- [66] B. Gurram, S. Zhang, M. Li, H. Li, Y. Xie, H. Cui, J. Du, J. Fan, J. Wang, X. Peng, *Anal. Chem.* **2018**, 90, 5187.
- [67] Y. Lou, P. C. McDonald, A. Oloumi, S. Chia, C. Ostlund, A. Ahmadi, A. Kyle, U. auf dem Keller, S. Leung, D. Huntsman, B. Clarke, B. W. Sutherland, D. Waterhouse, M. Bally, C. Roskelley, C. M. Overall, A. Minchinton, F. Pacchiano, F. Carta, A. Scozzafava, N. Touisni, J.-Y. Winum, C. T. Supuran, S. Dedhar, *Cancer Res.* **2011**, 71, 3364.
- [68] P.-C. Ho, J. D. Bihuniak, A. N. Macintyre, M. Staron, X. Liu, R. Amezcua, Y.-C. Tsui, G. Cui, G. Micevic, J. C. Perales, S. H. Kleinstein, E. D. Abel, K. L. Insogna, S. Feske, J. W. Locasale, M. W. Bosenberg, J. C. Rathmell, S. M. Kaech, *Cell* **2015**, 162, 1217.
- [69] S. J. Staffa, D. S. Kohane, D. Zurakowski, *Nano Lett.* **2021**, 21, 5457.
- [70] J. Foucquier, M. Guedj, *Pharmacol. Res. Perspect.* **2015**, 3, e00149.